# Solid-State Nuclear Magnetic Resonance Measurements of HIV Fusion Peptide ^{13}CO to Lipid ^{31}P Proximities Support Similar Partially Inserted Membrane Locations of the α Helical and β Sheet Peptide Structures

Charles M. Gabrys, Wei Qiang, Yan Sun, Li Xie, Scott D. Schmick, and David P. Weliky*

Department of Chemistry, Michigan State University, East Lansing, Michigan 48824, United States

S *Supporting Information*

ABSTRACT: Fusion of the human immunodeficiency virus (HIV) membrane and the host cell membrane is an initial step of infection of the host cell. Fusion is catalyzed by gp41, which is an integral membrane protein of HIV. The fusion peptide (FP) is the ~25 N-terminal residues of gp41 and is a domain of gp41 that plays a key role in fusion catalysis likely through interaction with the host cell membrane. Much of our understanding of the FP domain has been accomplished with studies of "HFP", i.e., a ~25-residue peptide composed of

the FP sequence but lacking the rest of gp41. HFP catalyzes fusion between membrane vesicles and serves as a model system to understand fusion catalysis. HFP binds to membranes and the membrane location of HFP is likely a significant determinant of fusion catalysis perhaps because the consequent membrane perturbation reduces the fusion activation energy. In the present study, many HFPs were synthesized and differed in the residue position that was ^{13}CO backbone labeled. Samples were then prepared that each contained a singly ^{13}CO labeled HFP incorporated into membranes that lacked cholesterol. HFP had distinct molecular populations with either α helical or oligomeric β sheet structure. Proximity between the HFP ^{13}CO nuclei and ^{31}P nuclei in the membrane headgroups was probed by solid-state NMR (SSNMR) rotational-echo double-resonance (REDOR) measurements. For many samples, there were distinct ^{13}CO shifts for the α helical and β sheet structures so that the proximities to ^{31}P nuclei could be determined for each structure. Data from several differently labeled HFPs were then incorporated into a membrane location model for the particular structure. In addition to the ^{13}CO labeled residue position, the HFPs also differed in sequence and/or chemical structure. "HFPmn" was a linear peptide that contained the 23 N-terminal residues of gp41. "HFPmn_V2E" contained the V2E mutation that for HIV leads to greatly reduced extent of fusion and infection. The present study shows that HFPmn_V2E induces much less vesicle fusion than HFPmn. "HFPtr" contained three strands with HFPmn sequence that were chemically cross-linked near their C-termini. HFPtr mimics the trimeric topology of gp41 and induces much more rapid and extensive vesicle fusion than HFPmn. For HFPmn and HFPtr, well-resolved α and β peaks were observed for A6-, L9-, and L12-labeled samples. For each of these samples, there were similar HFP ^{13}CO to lipid ^{31}P proximities in the α and β structures, which evidenced comparable membrane locations of the HFP in either structure including insertion into a single membrane leaflet. The data were also consistent with deeper insertion of HFPtr relative to HFPmn in both the α and β structures. The results supported a strong correlation between the membrane insertion depth of the HFP and its fusogenicity. More generally, the results supported membrane location of the HFP as an important determinant of its fusogenicity. The deep insertion of HFPtr in both the α and β structures provides the most relevant membrane location of the FP for HIV gp41-catalyzed membrane fusion because HIV gp41 is natively trimeric. Well-resolved α and β signals were observed in the HFPmn_V2E samples with L9- and L12- but not A6-labeling. The α signals were much more dominant for L9- and L12-labeled HFPmn_V2E than the corresponding HFPmn or HFPtr. The structural model for the less fusogenic HFPmn_V2E includes a shorter helix and less membrane insertion than either HFPmn or HFPtr. This greater helical population and different helical structure and membrane location could result in less membrane perturbation and lower fusogenicity of HFPmn_V2E and suggest that the β sheet fusion peptide is the most functionally relevant structure of HFPmn, HFPtr, and gp41.
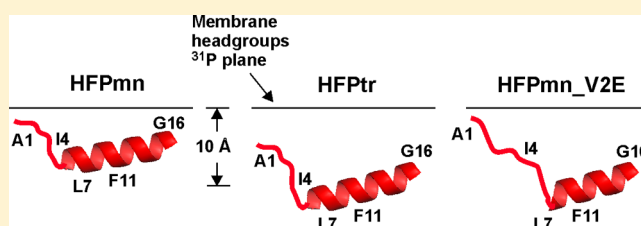
■ INTRODUCTION

Human immunodeficiency virus (HIV) is surrounded by a membrane taken from an infected host cell during viral budding. Infection of a new host cell begins with joining or "fusing" the HIV membrane with the host cell membrane to form a single membrane that encloses the cell and the viral

capsid.[1] Fusion is catalyzed by gp41, which is a HIV integral membrane protein. Gp41 includes a N-terminal ~170-residue ectodomain that lies outside the virus.[2] The ~25 N-terminal residues of the ectodomain are mostly apolar and are termed the fusion peptide (FP).[3,4] Point mutations in the FP often lead to reduced extent of gp41-catalyzed fusion and HIV infection, which supports the hypothesis that FP binding to the host cell membrane is a plausible early step of membrane fusion. Much of our understanding of the FP in gp41 is based on studies of the "HFP", which is a ~25-residue peptide containing the FP sequence and lacking most of the rest of gp41. The HFP binds to membranes and induces fusion of membrane vesicles.[5] There are typically good correlations between the effects of specific mutations on the rate and extent of HFP-induced vesicle fusion and the effects of these mutations on gp41-induced fusion and HIV infection.[4] The present study focuses on the structure and membrane location of the HFP. The results provide insight into the corresponding structure and membrane location of the FP during early steps of HIV/host cell fusion as well as how these FP properties aid fusion catalysis.

One of the constructs of the present study is HFPmn, which is a linear peptide composed of the 23 N-terminal residues of gp41 followed by non-native tryptophan as a 280 nm chromophore and a positively charged tag to improve aqueous solubility (Table 1). HFPmn induces vesicle fusion for a variety

Table 1. Sequences for HFPmn_V2E, HFPmn, and HFPtr[a,b]

Construct	Peptide Sequence
HFPmn	AVGIGALFLGFLGAAGSTMGARSWKKKKKA
HFPmn_V2E	AEGIGALFLGFLGAAGSTMGARSWKKKKKA
	AVGIGALFLGFLGAAGSTMGARSWKKKKKA
	|
HFPtr	AVGIGALFLGFLGAAGSTMGARSWKKKKC
	|
	AVGIGALFLGFLGAAGSTMGARSWKKKKCG

[a]The residues from W24 to the C-terminus are non-native. For all constructs, W24 provided a A_{280} chromophore and the positively charged lysines improved aqueous solubility. For HFPtr, the cysteines were used to cross-link the middle and lower peptide strands. [b]The line between K and C refers to an amide bond between the lysine ε-NH and the cysteine CO. The line between the two Cs refers to a disulfide bond.

of membrane compositions.[6] Previous studies probed the structures of detergent- and membrane-associated HFPmn as well as the locations of HFPmn in the detergent micelle or membrane bilayer.[7−18] Although membranes are fused by HFPmn, to our knowledge, detergent micelles are not fused by HFPmn.

The highest-resolution structures of detergent-associated HFPmn have been obtained from liquid-state NMR (LSNMR). The LSNMR data are consistent with α helical monomers with one report of a continuous α helix between residues 4 and 22.[10] The highest-resolution structural data for membrane-associated HFPmn have been obtained from solid-state NMR (SSNMR) with lower-resolution data from infrared and circular dichroism spectroscopies.[12,13,19−21] The HFPmn structure depends on the membrane composition. The membranes of host cells of HIV have ~0.3 mol fraction cholesterol and for this cholesterol fraction, HFPmn forms β sheet oligomers. There is antiparallel arrangement of adjacent HFPmn molecules and a mixture of antiparallel registries including populations of the A1→G16/G16→A1 registry and

the A1→S17/S17→A1 registry.[20] For membranes that lack cholesterol, a population of HFPmn molecules with oligomeric β sheet structure is observed as well as a separate population with α helical structure that are probably monomers.[14] For a sample prepared by freezing detergent-associated HFPmn, the SSNMR spectrum showed only the α helical population.[5] Therefore, the structural differences between detergent- and membrane-associated HFPmn appear to be genuinely environment-dependent rather than artifactually technique-dependent. HFPmn has random coil structure in aqueous solution that lacks detergent or lipids as evidenced by LSNMR of ambient temperature samples and SSNMR of frozen samples.[5]

For α helical HFPmn in detergent, the I4 to A15 region of the helix is likely inserted into the micelle interior.[7−10] For membrane-associated HFPmn with a F8W mutation and probably oligomeric β sheet structure, fluorescence data supported membrane insertion of the tryptophan and a distance of ~10 Å between the tryptophan indole group and the phosphate layer of the lipid headgroups.[22,23]

Extensive SSNMR studies were carried out on the location of HFPmn in membranes with ~0.3 mol fraction cholesterol for which there was a single population of HFPmn with β sheet structure.[15] For each SSNMR sample, the HFPmn had a single [13]CO label in the peptide backbone and the [13]CO region of the ^{13}C SSNMR spectrum was dominated by signal from these labeled [13]CO nuclei. The rotational-echo double-resonance (REDOR) SSNMR method was applied to detect <12 Å contact between the labeled [13]CO nucleus and the ^{31}P nuclei of the membrane headgroups.[24−26] Complementary [13]CO−[19]F REDOR measurements were done using samples for which ~0.1 fraction of the membrane lipids was dipalmitoylphosphatidylcholine (DPPC) "chemically labeled" with a [1]H→[19]F substitution at either the C5 (DPPC-F5) or C16 (DPPC-F16) position of the palmitic acid chains.[27,28] The REDOR measurements detected contact between the labeled HFPmn [13]CO nucleus and the lipid ^{19}F nuclei. For the DPPC-F16 sample, the ^{19}F nuclei were located near the membrane center. For the DPPC-F5 sample, the ^{19}F nuclei were located midway between the membrane center and the ^{31}P nuclei of the membrane headgroups. There is ~20 Å distance along the membrane normal between the bilayer center and these ^{31}P nuclei.[29]

Besides the distinction between DPPC-F5 and DPPC-F16 lipids, the samples also differed in the residue position of the [13]CO label in HFPmn. Analysis of [13]CO−[31]P and [13]CO−[19]F REDOR data for many different samples led to an experimentally based membrane location model of oligomeric antiparallel β sheet HFPmn. The residues near the ends of the β sheet, e.g., A1 and A14, were in close (van der Waals) contact with the phosphate groups whereas the residues on the interior of the β sheet, e.g., A6 and L9, were in contact with the ^{19}F nuclei of the DPPC-F5 samples. Overall, the analysis supported insertion of the most apolar A6 to L12 region of the β sheet into the hydrocarbon core of a single membrane leaflet with the more polar ends of the β sheet in the headgroup region of the membrane. Further support for insertion was provided by [13]CO−[2]H REDOR on a sample containing β sheet HFPmn with a F8 [13]CO label and lipids with perdeuterated acyl chains.[30] Large [13]CO−[2]H REDOR contact was consistent with proximity between HFPmn F8 and some of the −CD_2− and/or −CD_3 groups in the membrane core.

For both this earlier and the present study, two HFP variants were studied in addition to HFPmn (Table 1). The HFPmn_V2E peptide was the same as HFPmn except for the V2E point mutation. Relative to HIV with the wild-type FP, HIV with this FP mutation is much less fusogenic and infectious.[31] Relative to 23-residue wild-type HFP, HFP with the V2E mutation is also much poorer at catalyzing vesicle fusion.[19] In the present study, vesicle fusion is assayed in the presence of either HFPmn or HFPmn_V2E (both with non-native charged residues to improve aqueous solubility) and much less fusion extent is observed with HFPmn_V2E. HFPtr is the other HFP construct studied and contains three HFPmn peptides that are chemically cross-linked in their C-terminal regions.[6] The gp41 protein is a trimer and the trimeric topology of HFPtr is the likely FP topology of gp41 during some steps of HIV/host cell fusion.[1,32] Relative to HFPmn, HFPtr induces vesicle fusion with ~40 times faster rate when the vesicle membranes contained ~0.3 mol fraction cholesterol and ~15 times faster rate when the vesicle membranes lacked cholesterol.[6] The rates were compared for the same concentrations of peptide strands, i.e., [HFPtr] = [HFPmn]/3.

For membranes with cholesterol, the ^{13}CO spectra of HFPtr were similar to those of HFPmn and showed a single conformational population with β sheet structure.[15] The spectra of HFPmn_V2E showed predominant β sheet structure although there was often a higher ^{13}CO shift shoulder that was assigned to a minor α helical population. The $^{13}CO-^{31}P$ and $^{13}CO-^{19}F$ REDOR data were consistent with deeper membrane insertion of HFPtr relative to HFPmn and with shallower membrane insertion of HFPmn_V2E relative to HFPmn. Overall, these data for oligomeric β sheet HFPs in membranes with cholesterol supported a strong positive correlation between the depth of HFP membrane insertion and the magnitude of fusion catalysis. Deep HFP insertion into a single membrane leaflet would likely perturb the surrounding lipid molecules and make the local lipid structure look more like the fusion transition state, thereby reducing the activation energy for fusion. The fusion transition state likely contains regions of high membrane curvature, and experimental data from SSNMR and other methods support a reduced bending modulus for the membrane in the presence of HFP.[33,34] The equilibrium membrane bilayer structure remains intact with HFP:lipid mole ratio of 0.1, which is consistent with expected evolutionary pressure for a viable host cell.[33]

For the present study, the sample preparation and SSNMR approaches to probe HFP membrane location are similar to those of the earlier SSNMR study except for the absence of cholesterol in the membranes of the present study. This absence resulted in distinct populations of α helical and β sheet HFPmn. Because the SSNMR signals of ^{13}CO nuclei in α helices are often resolved from those in β sheets, the present study allowed us to develop membrane location models for α helical HFPmn, HFPmn_V2E, and HFPtr. Knowledge of these locations is important because there is not yet a consensus in the literature about the fusion-active conformation of HFP. Different literature data suggest that this conformation is (1) α helix, (2) β sheet, (3) both α helix and β sheet, or (4) random coil.[6,12,19,35,36]

In addition, the results provide information about the effect of cholesterol on β sheet HFP membrane location, allow comparison between the membrane locations of the α helix vs β sheet HFP, and give insight into the relative effects of HFP conformation and sequence on membrane location. The SSNMR location data for the α helical HFP in membranes is also compared to the LSNMR-determined model of the location of a single α helical HFP molecule in a detergent micelle. The location data should be useful to constrain simulations of HFPs in membranes. To date, there are very different simulation results from different groups and approaches about the membrane location of a single α helical HFP molecule in membranes with reports of both surface and transmembrane locations.[37−39] To our knowledge, there are not yet simulations of oligomeric β sheet HFP molecules in membranes.

■ EXPERIMENTAL METHODS

Peptides. Table 1 displays the primary sequences for HFPmn, HFPmn_V2E, and HFPtr. Peptide syntheses were done manually using resins and amino acids that were purchased from Peptides International (Louisville, KY). ^{13}CO-labeled amino acids were obtained from Cambridge Isotope Laboratories (Andover, MA). HFPmn and HFPmn_V2E were synthesized and purified using the same published protocol, and HFPtr was synthesized by a separate protocol.[14] Purified peptides were identified with mass spectrometry.

Intervesicle Lipid Mixing. Vesicle fusion induced by either HFPmn or HFPmn_V2E was assayed by an increase in fluorescence due to intervesicle lipid mixing.[5] Such mixing has also been observed in membrane fusion induced by intact HIV proteins.[40] Briefly, a solution was prepared that contained two populations of vesicles. The minor "labeled" vesicle population contained a small fraction of fluorescent lipid and a small fraction of quenching lipid and the major "unlabeled" population contained neither fluorescent nor quenching lipids. Fusion between a labeled vesicle and an unlabeled vesicle increased the average fluorophore/quencher distance with consequent increased fluorescence. The fluorescence reference value F_0 was measured for the vesicle solution prior to addition of an aliquot of HFP solution at time $t \approx 0$. Over the next 600 s, the fluorescence $F(t)$ was measured every 1 s. An aliquot of Triton X-100 detergent was then added to the HFP/vesicle solution to dissolve the vesicles with consequent large increase in fluorophore/quencher distance and maximum fluorescence F_{max}. The percent lipid mixing $= 100 \times \{F(t) - F_0\}/\{F_{max} - F_0\}$.

The assays were done at 30 °C in 5 mM N-(2-hydroxyethyl)piperazine-N'-2-ethanesulfonic acid (HEPES) buffer with pH 8. Unilamellar vesicles of ~100 nm diameter were formed from extrusion of a lipid suspension. The unlabeled vesicles contained 1-palmitoyl-2-oleoyl-sn-glycero-3-phosphocholine (POPC), 1-palmitoyl-2-oleoyl-sn-glycero-3-[phospho-(1′-rac-glycerol)] (POPG), and cholesterol. [POPC] = 120 μM, [POPG] = 30 μM, and [cholesterol] = 75 μM. The labeled vesicles contained additional N-(7-nitro-2,1,3-benzoxadiazol-4-yl)-dipalmitoylphosphatidylethanolamine (N-NBD-PE) fluorescent lipid and N-(lissamine Rhodamine B sulfonyl)-dipalmitoylphosphatidylethanolamine (N-Rh-PE) quenching lipid with [N-NBD-PE] = [N-Rh-PE] = 3 μM. The ratio [unlabeled vesicle]/[labeled vesicle] = 9. There was continuous excitation and fluorescence detection of N-NBD-PE at 465 and 530 nm, respectively. [HFP] = 3 μM. Different trials of this assay have typical ±2% variation in long-time lipid mixing.[5]

Preparation of SSNMR Samples. The lipids were 1,2-di-O-tetradecyl-sn-glycero-3-phosphocholine (DTPC), 1,2-di-O-tetradecyl-sn-glycero-3-[phospho-(1′-rac-glycerol)] (DTPG),

and 1-palmitoyl-2-(16-fluoropalmitoyl)-sn-glycero-3-phospho-choline (DPPC-F16), all purchased from Avanti (Alabaster, AL). Each sample contained 32 μmol of DTPC, 8 μmol of DTPG, and 4 μmol of DPPC-F16. The choices of phosphocholine and phosphoglycerol lipids respectively reflect the significant fraction of phosphatidylcholine lipids and some negatively charged lipids in the membranes of host cells of HIV.[41] DTPC and DTPG were used because they are ether-linked rather than ester-linked lipids and lack carbonyl carbons. The ^{13}CO region of the NMR spectrum was therefore dominated by the labeled ^{13}CO nucleus of the HFP. The DPPC-F16 lipids were included for HFP ^{13}CO–lipid ^{19}F REDOR experiments to probe the residue proximity to the middle of the bilayer. The results of these ^{13}CO–^{19}F experiments are not discussed because the spectral signal-to-noise was too low to provide information about this proximity.

HFPmn_V2E (0.80 μmol), HFPmn (0.80 μmol), or HFPtr (0.27 μmol) was dissolved in 30 mL of 5 mM HEPES buffer at pH 7. The HFP solution was added dropwise to 4 mL of vesicle suspension and after overnight mixing, the suspension was centrifuged at 150000g for 4 h. The resultant pellet contained membrane-associated HFP because unbound HFPs do not pellet under these centrifugation conditions.[6] HFPmn binds quantitatively to membranes with a fraction of negatively charged lipid so the HFP strand:lipid ratio was ~0.018 for all samples. The pellet was lyophilized, transferred to a 4 mm diameter magic angle spinning (MAS) SSNMR rotor, and rehydrated with 10 μL HEPES buffer.

REDOR Experiments and Data Analysis. A full description of the ^{13}CO–^{31}P REDOR experiments has been previously published so only an abbreviated description is provided here.[14−16] The data were acquired with a 9.4 T spectrometer and ^1H/^{31}P/^{13}C triple resonance probe, 8 kHz MAS frequency, and sample cooling with nitrogen gas at −50 °C with a consequent sample temperature of ~−30 °C. The SSNMR signal-to-noise is greater at lower temperature and a membrane-associated HFP has very similar structures at ambient and lower temperatures. The samples likely contain gel phase membranes.[16] The ^{13}CO–^{31}P REDOR data were two separate acquisitions denoted "S_0" and "S_1". The time sequence of REDOR included: (1) generation of ^{13}C transverse magnetization with a 50 kHz ^1H $\pi/2$ pulse and 1 ms of cross-polarization with a 52 kHz ^1H field and a 58−69 kHz ramped ^{13}C field; (2) dephasing period of duration τ with a 50 kHz ^{13}C π pulse at the end of each rotor cycle except the last cycle and, for the S_1 acquisition only, a 60 kHz ^{31}P π pulse at the midpoint of each rotor cycle; and (3) ^{13}C detection followed by 1 or 2 s recycle delay. ^1H decoupling at 100 kHz was applied during the dephasing and detection periods. Spectral processing included Gaussian line broadening and baseline correction. Indirect ^{13}C referencing was done using the methylene resonance of adamantane at 40.5 ppm so that the referenced ^{13}C shifts could be directly compared to those of ^{13}C spectra in the liquid state.[17]

The REDOR data provide information about the proximity of a labeled HFP ^{13}CO to nearby lipid ^{31}P nuclei with a distance (r) detection range of $r \leq 12$ Å.[24] During the dephasing period of a S_0 acquisition, the evolution of the ^{13}CO transverse magnetization due to ^{31}P dipolar fields is refocused at the end of each rotor period. During the dephasing period of a S_1 acquisition, there is evolution due to these fields and relative to S_0, there is consequent reduction in the S_1 ^{13}CO signal intensity. The fractional reduction typically becomes

larger with increased dephasing time τ. The integrated ^{13}CO signal intensities of the S_0 and S_1 spectra were also denoted S_0 and S_1. The experimental fractional dephasing $(\Delta S/S_0)^{exp} = (S_0 − S_1)/S_0$ was calculated for each sample and each τ, and the buildup of $(\Delta S/S_0)^{exp}$ vs τ for the sample provided information about the labeled HFP ^{13}CO to lipid ^{31}P proximities.

There were two approaches for integration of spectral intensities. One approach was applied to all spectra and was integration over the full ^{13}CO region (typically an interval of ~7 ppm). Some of the spectra had two resolved peaks and the peaks at higher and lower chemical shift corresponded to HFP populations with respective α helical and β sheet structure. For these spectra, S_0 and S_1 intensities were determined with 2 ppm integration windows centered at either the α or β peak shift. The uncertainty in each $(\Delta S/S_0)^{exp}$ was calculated using the experimental spectral noise.[17]

■ RESULTS

Vesicle Fusion. Figure 1 displays the time courses of vesicle fusion induced by either HFPmn or HFPmn_V2E. HFPmn
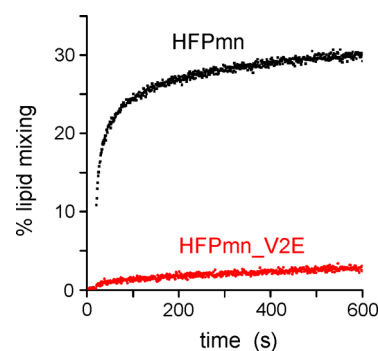
Figure 1. Membrane vesicle fusion induced by either HFPmn (black trace) or HFPmn_V2E (red trace) with [HFP]:[total lipid] = 0.02. As detailed in the Experimental Methods, percent lipid mixing was calculated from lipid fluorescence. The peptide was added at 20 s and there was ~5 s dead time in the assay during this addition. This dead time accounts for the discontinuity in the data around 20 s.

induces much faster vesicle fusion than HFPmn_V2E as well as 10 times greater long-time fusion extent. The observation of much more rapid and extensive fusion for HFPmn relative to HFPmn_V2E is similar to previous results for other peptides which lacked the C-terminal lysine tag.[19] The observation also correlates with much higher fusion and infection of HIV with wild-type FP compared to HIV with the V2E mutation.[31] All of these data support the catalytic significance of the N-terminal FP sequence of gp41.

S_0 REDOR Spectra. Figure 2 displays the ^{13}CO regions of the S_0 and S_1 REDOR spectra at 24 ms dephasing time. Figure S1 in the Supporting Information displays the S_0 and S_1 spectra over the full ^{13}C shift range for the "HFPmn-L9" sample, i.e., the sample containing HFPmn labeled at L9. For a given sample, the S_0 spectra at other dephasing times have similar line shapes. The natural abundance (na) contributions of lipid DPPC-F16 ^{13}CO nuclei to the displayed S_0 spectra are not considered because these nuclei have shorter transverse relaxation times (T_2) than the HFP ^{13}CO nuclei.[30] Spin counting yields a ~0.75 fractional contribution of the labeled (lab) ^{13}CO nucleus to the ^{13}CO S_0 intensity and a ~0.25 na contribution distributed among the 30 unlabeled HFP CO sites. The T_2 of the HFP ^{13}CO nuclei is ~15 ms with
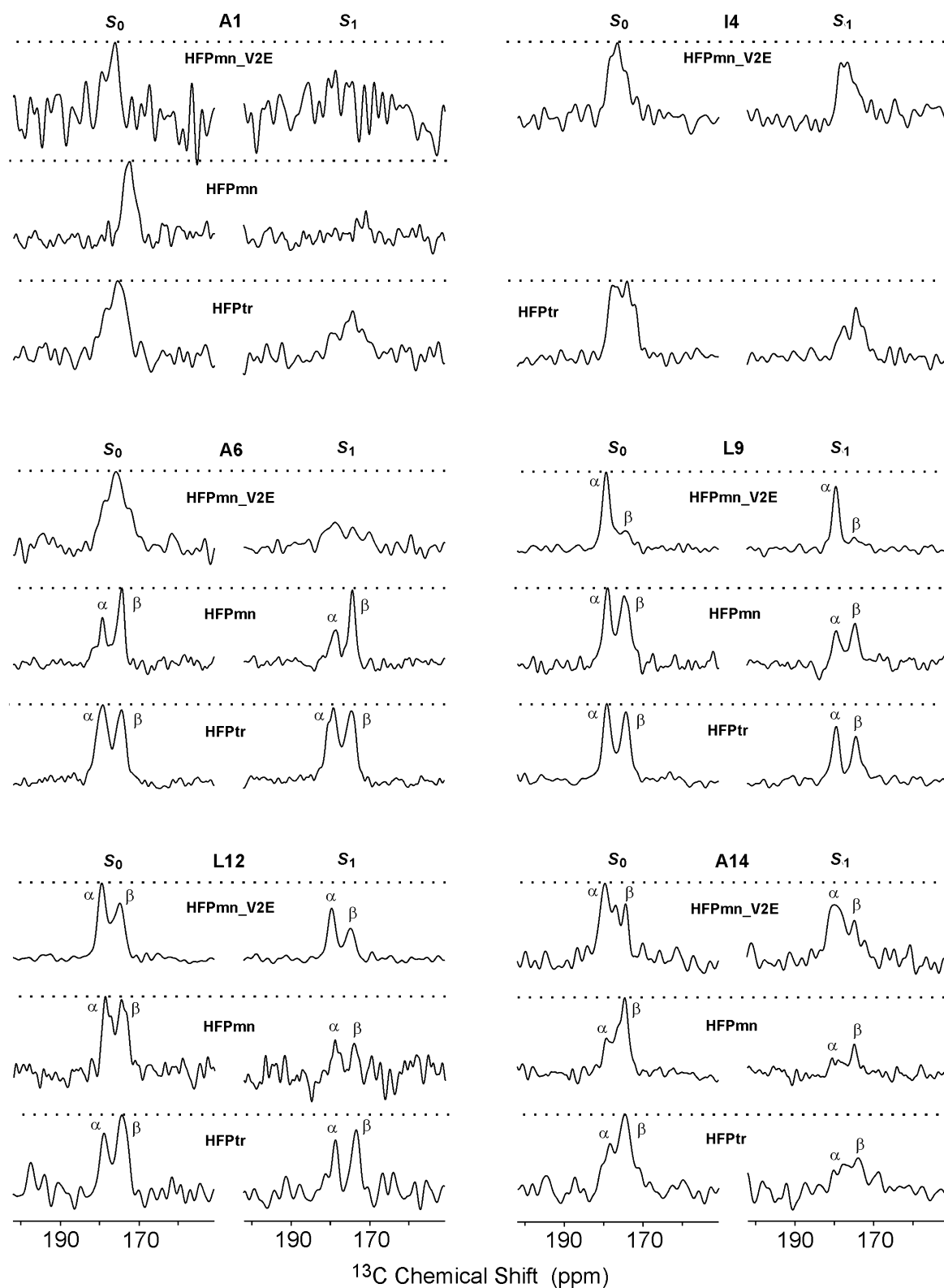
Figure 2. ^{13}CO region of the $^{13}C-^{31}P$ REDOR spectra at 24 ms dephasing time of samples containing either HFPmn_V2E, HFPmn, or HFPtr. The spectra were scaled to have about the same vertical intensity for the most intense peak in the S_0 spectrum. The α and β identify peaks associated with populations of HFP molecules with either α helical or β sheet structure at the labeled residue. This identification is based on peak ^{13}CO shift. For a few samples, only a single broad peak was observed so the α/β identification was not done. Spectra were processed with 100 Hz Gaussian line broadening and baseline correction. For each S_0 and S_1 spectrum of a sample containing HFPmn_V2E with a specific (^{13}CO labeled residue), the numbers of acquisitions summed were as follows: (A1) 9784; (I4) 10000; (A6) 27345; (L9) 2278; (L12) 10000; and (A14) 19582. Numbers for HFPmn: (A1) 25168; (A6) 12160; (L9) 24704; (L12) 20864; (A14) 20000. Numbers for HFPtr: (A1) 26240; (I4) 26240; (A6) 20736; (L9) 17192; (L12) 23907; and (A14) 23442. No spectra were collected for HFPmn labeled at I4.

Table 2. ^{13}CO Peak Chemical Shifts^{a}

	^{13}CO labeled residue					
peptide	A1	I4	A6	L9	L12	A14
HFPmn_V2E	175.9	176.9	175.2	179.7, 175.3	179.4, 175.3	180.1, 175.8
HFPmn	173.5		179.5, 174.7	179.3, 174.8	179.1, 175.2	179.4, 175.4
HFPtr	175.1	177.8, 174.7	179.3, 174.6	179.4, 174.7	179.3, 174.8	179.2, 175.5

^{a}For each labeled sample, the S_0 spectra at all dephasing times were examined and it was decided whether to interpret the spectra with one or two peaks. For either the one peak or for each of the two peaks, the ^{13}CO peak shifts from spectra of all dephasing times were averaged and this average shift is listed. Comparison of spectra for all dephasing times typically showed a 0.4 ppm difference between the largest and smallest peak shifts.

consequent ~0.2 ppm homogeneous contribution to the full-width at half-maximum (FWHM) S_0 ^{13}CO line width.[18] This contribution is much less than the 2−8 ppm experimental S_0 ^{13}CO line widths in Figure 2 so these line widths are primarily ascribed to inhomogenous broadening, i.e., the distribution of ^{13}CO shifts of the labeled ^{13}CO nuclei. The shift distribution reflects structural variation near the labeled site for the different HFP molecules in the sample.

For some samples, the S_0 spectra have two resolved peaks, most notably the A6-labeled HFPmn and HFPtr samples, and the L9- and L12-labeled HFPmn_V2E, HFPmn, and HFPtr samples. The typical higher peak ^{13}CO shift is in the 179−180 ppm range and the lower peak shift is in the 174.5−175.5 ppm range (Table 2). These higher and lower shift peaks are respectively assigned to populations of HFP molecules with either monomeric α helical or oligomeric β sheet structure near the labeled site. The α helical assignments are based in part on earlier LSNMR studies of HFPmn in detergent.[10,11] These studies showed HFPmn monomers and α helical structure at A6, L9, and L12 with respective ^{13}CO shifts of 181.2, 180.5, and 179.1 ppm. Further support for the α helical assignments was from earlier SSNMR spectra of HFPtr associated with membranes without cholesterol.[17] The L7 ^{13}CO peak shift was 178.8 ppm, the F8 ^{13}CO peak shift was 178.4 ppm, and the REDOR-determined L7 ^{13}CO-F11 ^{15}N distance of 4.1 ± 0.1 Å agreed quantitatively with the residue i ^{13}CO to residue $i + 4$ ^{15}N distance of regular α helical structure. The β sheet peak assignments of Figure 2 and Table 2 are based in part on earlier SSNMR studies of HPFmn associated with membranes with cholesterol.[13,20] These studies showed HFPmn oligomers and intermolecular antiparallel β sheet structure at A6, L9, and L12 with respective ^{13}CO peak shifts of 174.2, 174.7, and 174.4 ppm. For HFPtr in membranes with cholesterol, the L7 and F8 ^{13}CO peak shifts were respectively 173.8 and 172.5 ppm and the L7 ^{13}CO-F11 ^{15}N REDOR data were consistent with oligomeric antiparallel β sheet structure of the HFP strands and were not consistent with α helical structure.[17] These HFPtr β sheet shifts were 5−6 ppm lower than the corresponding shifts of α helical HFPtr in membranes without cholesterol. For the present study, the β sheet shift of an A6, L9, or L12 sample was also typically 4−5 ppm lower than the corresponding α helical shift. The typical FWHM line width for either the α or β peak is 3 ppm (Table 3), which is comparable to the typical line widths of the single peaks of β sheet HFP in membranes with cholesterol.[15]

The Figure 2 spectra of the A14 labeled samples appear less well-resolved than those of the A6, L9, and L12 labeled samples. It was still usually possible to identify two peaks in these A14 spectra with associated shifts of ~179.5 and ~175.5 ppm. The higher shift is similar to the A14 ^{13}CO shift of 179.3 ppm for monomeric α helical HFPmn in detergent micelles and

**Table 3. Full-Width at Half-Maximum Line Widths of S_0 ^{13}CO Spectra^{a}**

peptide	labeled residue	total peak	α peak	β peak
HFPmn_V2E	A1	5.1		
	I4	4.9		
	A6	6.3		
	L9^{b}	2.1		
	L12	6.7	2.4	2.9
	A14	7.4	3.0	1.7
HFPmn	A1	3.4		
	A6	6.3	1.7	1.8
	L9	7.1	2.1	3.5
	L12	6.7	2.9	3.1
	A14^{c}	2.8		
HFPtr	A1	6.5		
	I4	7.8		
	A6	7.6	3.5	3.3
	L9	7.1	2.2	2.5
	L12	7.4	2.3	3.9
	A14	6.3		3.3

^{a}The line widths were typically measured from the S_0 spectrum with 24 ms dephasing time that had been processed with 50 Hz Gaussian line broadening. The estimated measurement uncertainty is ±0.2 ppm. For some spectra, the minimum intensity between the α and β peaks was greater than half the maximum α peak intensity. For these cases, the half-width at half-maximum (HWHM) of the α peak was measured using the half-maximum intensity to higher shift. The table entry is then 2 × HWHM. A similar approach was applied when the minimum intensity between the α and β peaks was greater than half the maximum β peak intensity. ^{b}The spectrum of HFPmn_V2E-L9 sample is approximately a single peak with shift corresponding to α helical structure. ^{c}The spectrum of HFPmn-A14 sample is approximately a single peak with shift corresponding to β sheet structure.

the lower shift is similar to the 174.9 ppm shift for oligomeric antiparallel β sheet HFPmn in membranes with cholesterol. The S_0 spectra of the A1 and I4 labeled samples typically show single peaks with FWHM line widths of 4−7 ppm. These spectra indicate structural heterogeneity near the HFP N-terminus.

The S_0 spectra of the L9, L12, and A14 labeled samples all show a larger α helical:β sheet peak intensity ratio for HFPmn_V2E than for HFPmn or HFPtr. This intensity ratio should approximately correlate with the α helical:β sheet molecular population ratio. The construct-dependent difference in α:β ratio is clearest in the L9 spectra for which the α:β peak intensity ratio is ~4.2 for HFPmn_V2E and ~1.1 for HFPmn and HFPtr. Interestingly, relative to HFPmn and HFPtr, larger α:β peak intensity ratios have also been observed for HFPmn_V2E in membranes with cholesterol.[15] For example, for L9-labeled samples in membranes with cholesterol, the α:β
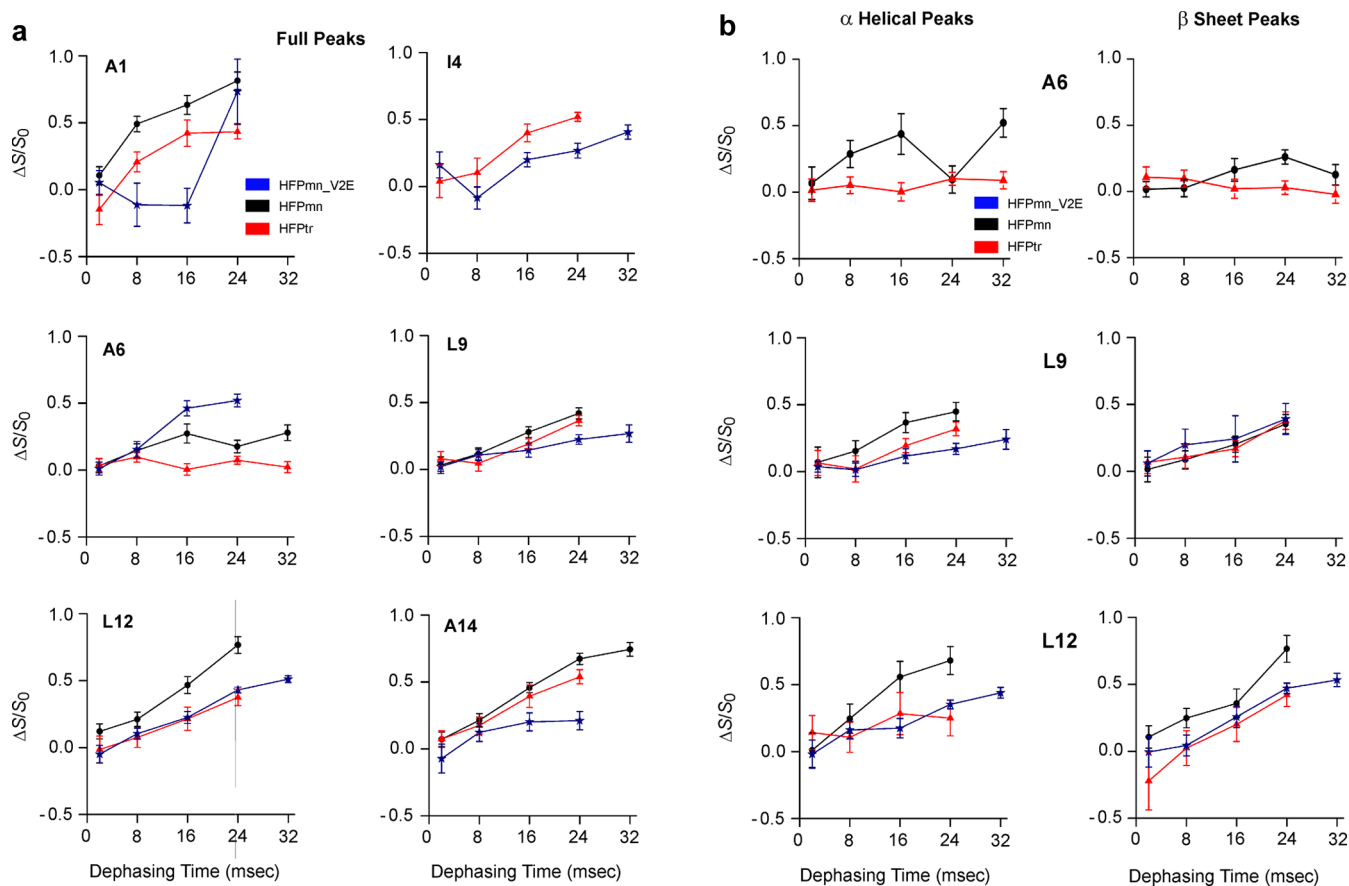
Figure 3. Plots of experimental $\Delta S/S_0$ vs dephasing time for the HFP samples. For panel a, the S_0 and S_1 intensities were integrated over the full ^{13}CO peak region. Panel b displays plots for samples for which there were well-resolved α helical and β sheet peaks. For panel b, the S_0 and S_1 intensities were integrated in 2 ppm windows centered at the peak shifts. The displayed $\pm 1\sigma$ standard deviations were calculated on the basis of the spectral noise. The spectra had been processed with 200 Hz Gaussian line broadening and baseline correction. The Figure 2 caption provides typical numbers of scans summed for a spectrum.

peak intensity ratio was ~0.4 for HFPmn_V2E and ~0 for HFPmn and HFPtr. HFPmn_V2E is the least fusogenic construct (Figure 1), so these results suggest that α helical HFP may be less fusogenic than β sheet HFP.

Figure 2 and Table 3 show that the S_0 spectra of the HFPmn-A6, HFPmn-L9, HFPtr-A6, and HFPtr-L9 samples have well-resolved α helical and β sheet peaks with line widths of ~3 ppm and $\alpha{:}\beta$ peak intensity ratios of ~1. As noted above, the spectrum of the HFPmn_V2E-L9 sample is dominated by a sharp α helical peak with ~2 ppm line width. The spectrum of the HFPmn_V2E-A6 sample is different and has a single broad feature with 6.3 ppm line width. The spectral breadth of HFPmn_V2E-A6 relative to the other samples suggests that the V2E mutation interferes with formation of regular α helical structure near the HFP N-terminus.

^{13}CO−^{31}P REDOR Dephasing. Figure 3 displays plots of $(\Delta S/S_0)^{exp}$ vs dephasing time τ. For panel a, the S_0 and S_1 intensities were integrated over the full ^{13}CO peak region whereas in panel b, the intensities were integrated over 2 ppm intervals centered at either the α helical or β sheet peak shifts. The panel b plots were only done for samples for which there were clearly resolved α helical and β sheet peaks, i.e., all L9 and L12 samples, and the HFPmn-A6 and HFPtr-A6 samples. The data typically have insufficient signal-to-noise and number of τ values for quantitative determination of the distribution of ^{13}CO−^{31}P distances. One reason for relatively low signal-to-

noise is the spectral breadth, which reflects significant populations of both α helical and β sheet HFPs.

Semiquantitative analysis of the experimental $(\Delta S/S_0)^{exp}$ vs τ is based on the simulated $(\Delta S/S_0)^{sim}$ vs τ for a single ^{13}CO−^{31}P spin pair separated by distance r.[24] $(\Delta S/S_0)^{sim}$ is characterized by a parameter $\lambda = (\tau \times 12244/r^3)$ with τ in s and r in Å. $(\Delta S/S_0)^{sim}$ increases with λ and some reference values include $(\Delta S/S_0)^{sim} \approx 0.1$ for $\lambda \approx 0.2$, $(\Delta S/S_0)^{sim} \approx 0.5$ for $\lambda \approx 0.7$, and $(\Delta S/S_0)^{sim} \approx 1$ for $\lambda \approx 1.5$. $(\Delta S/S_0)^{sim}$ remains ~1 for $\lambda > 1.5$.

The labeled (lab) ^{13}CO nucleus makes ~0.75 fractional contribution to the integrated S_0 intensity with the remainder dispersed among the na ^{13}CO sites of the 29 unlabeled residues. $(\Delta S/S_0)^{exp} \approx [0.75 \times (\Delta S/S_0)^{lab}] + [0.25 \times (\Delta S/S_0)^{na}]$ and for a particular construct and τ value, $(\Delta S/S_0)^{na}$ is approximated as the average of the $(\Delta S/S_0)^{exp}$ of all labeled samples. If a particular sample has $(\Delta S/S_0)^{lab} > (\Delta S/S_0)^{na}$, it is therefore expected that $(\Delta S/S_0)^{exp} < (\Delta S/S_0)^{lab}$ whereas for $(\Delta S/S_0)^{lab} < (\Delta S/S_0)^{na}$, it is expected that $(\Delta S/S_0)^{exp} > (\Delta S/S_0)^{lab}$. These inequalities are generally supported by the data in Figure 3a where the maximal $(\Delta S/S_0)^{exp} \approx 0.8$ rather than 1 (for HFPmn-A1 at $\tau = 24$ ms) and nearly all the samples have some buildup of $(\Delta S/S_0)^{exp}$ as τ increases.

For some of the $(\Delta S/S_0)^{exp}$ plots, the labeled ^{13}CO−^{31}P distances are semiquantitatively assessed using the single spin pair model. For the HFPmn-A1 sample at $\tau = 24$ ms, we approximate that $(\Delta S/S_0)^{exp} \approx 0.8$ with full peak integration

translates to $(\Delta S/S_0)^{lab} \approx 1$ with corresponding $\lambda \approx 1.5$ and calculated $r \approx 5.8$ Å. This distance is consistent with close contact between the A1 residue and the phosphates of the lipid head groups. This contact is likely due to the electrostatic attraction between the positively charged N-terminal amino group and the negatively charged phosphates. The robustness of the $(\Delta S/S_0)^{exp}$ data and distance analysis is supported by the close similarities between the $(\Delta S/S_0)^{exp}$ and derived r and those previously obtained for HFPmn-A1 in membranes with cholesterol.[15] Relative to HFPmn-A1, the $(\Delta S/S_0)^{exp}$ buildup of HFPtr-A1 in membranes without cholesterol has a similar shape and smaller maximal value, which indicates that at least a significant fraction of the A1 residues of HFPtr are in close contact with the negatively charged phosphate groups. The spectra of the HFPmn_V2E sample have lower signal-to-noise (Figure 2) but appear to have slower $(\Delta S/S_0)^{exp}$ buildup and greater r than HFPmn-A1. This may be due to electrostatic repulsion between the E2 carboxylate and the phosphate groups.

The HFPtr-A6 sample shows very different $(\Delta S/S_0)^{exp}$ than HFPmn-A1. For HFPtr-A6, $(\Delta S/S_0)^{exp} \leq 0.1$ for all τ for both the α helical and β sheet peaks, Figure 3b, and these inequalities are also true for the full peak integrations, Figure 3a. For $\tau = 32$ ms, we correlate $(\Delta S/S_0)^{exp} \leq 0.1$ to $(\Delta S/S_0)^{lab} \leq 0.1$ and $\lambda \leq 0.2$ with consequent $r \geq 12$ Å. This result is consistent with insertion of the A6 residue of HFPtr into the hydrocarbon core of the membrane. Membrane rather than aqueous location is chosen because of the hydrophobicity of the HFP sequence. This insertion is for both the α helical and the β sheet HFPtr populations. The robustness of the $(\Delta S/S_0)^{exp}$ data is supported by the very similar $(\Delta S/S_0)^{exp} \leq 0.1$ previously observed for HFPtr-A6 in membranes with cholesterol.[15] For this membrane composition, there are only β sheet HFPtr.

Similar Membrane Locations of α Helical and β Sheet HFPs. Figure 3b was used to compare the $(\Delta S/S_0)^{exp}$ data for the α and β peaks of the same A6-, L9-, or L12-labeled sample. For most samples, the $(\Delta S/S_0)^{exp}$ were similar for the α and β peaks. This was noted above for HFPtr-A6 and is also clear for HFPtr-L9, HFPmn_V2E-L9, and HFPmn-L12 as well as other samples. These similarities support comparable membrane locations of a given HFP construct in both the α helical and β sheet structures. This conclusion only has direct experimental support for the well-structured A6-L12 regions of HFPmn and HFPtr and the well-structured L9-L12 region of HFPmn_V2E.

Deeper Membrane Insertion of HFPtr than HFPmn. Comparison was made between the $(\Delta S/S_0)^{exp}$ data for HFPmn and HFPtr samples that were labeled at the same site, Figure 3. For equivalently labeled HFPmn and HFPtr at each τ value, $(\Delta S/S_0)^{HFPmn} \geq (\Delta S/S_0)^{HFPtr}$ for both the full line width measurements of Figure 3a and the α and β peaks of Figure 3b. These results support deeper membrane insertion of HFPtr for both the α helical and β sheet structures. $(\Delta S/S_0)^{HFPmn\_V2E} \approx (\Delta S/S_0)^{HFPtr} \leq (\Delta S/S_0)^{HFPmn}$ for the α peaks of the L9 and L12 labeled samples and also for the β peaks of these samples. HFPmn_V2E has a much larger α:β population ratio than HFPmn and HFPtr. This complicates comparison of the full peak $(\Delta S/S_0)^{HFPmn\_V2E}$ with the full peak $(\Delta S/S_0)^{HFPmn}$ and $(\Delta S/S_0)^{HFPtr}$ for the other labeled samples for which the α and β peaks are not well-resolved.

Membrane Location Models. Figure 4 displays membrane location models based on the HFP ^{13}CO-lipid ^{31}P $(\Delta S/S_0)^{exp}$ data. Models are displayed for the α helical and β sheet HFPmn and HFPtr and for α helical HFPmn_V2E. No model
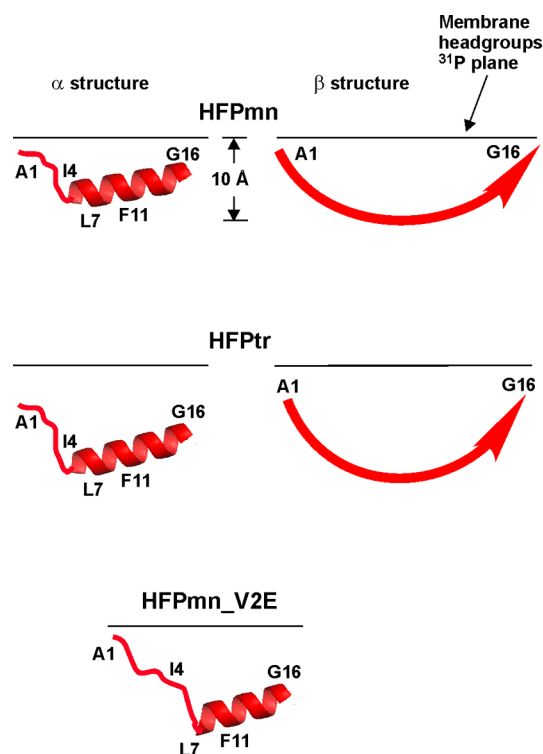
Figure 4. Models of HFP backbone structures and locations in membranes without cholesterol. Each black line represents one of the planes of the ^{31}P nuclei of the membrane headgroups. The longitudinal distance between this plane and the membrane bilayer center is ~20 Å. The backbone HFP ribbons extend between residues A1 and G16, the α helices of HFPmn and HFPtr extend from I4 to G16, and the α helix of HFPmn_V2E extends from L7 to G16. There are approximately equal populations of α and β structures for HFPmn and HFPtr whereas there is dominant α population for HFPmn_V2E. The approximate locations of a few different residues are displayed.

was developed for β sheet HFPmn_V2E because HFPmn_V2E-L12 was the only HFPmn_V2E sample with a significant resolved β sheet signal. The models show ribbon representations of residues 1−16 of a single HFP molecule. This residue choice was based on labeling between residues 1 and 14 and earlier studies showing a significant fraction of β sheet HFPmn with antiparallel registry A1→G16/G16→A1.[20] We do not show the additional HFP molecules in the β sheet. We also do not show the trimerization of either α helical or β sheet HFPtr.

The black line in each model represents one of the planes of ^{31}P nuclei of the phosphate headgroups of the membrane. The models are based on a flat plane of lipid molecules but there are likely local perturbations of the plane in the vicinity of the HFP. There is SSNMR evidence for global retention of membrane bilayer phase in the presence of 0.1 mol fraction HFP.[33] For HFPmn and HFPtr, the α helix begins at I4 and this choice is based on the LSNMR structures of HFPmn in detergent.[10,12] We note that one of these structures shows contiguous extension of the helix to residue 22.[10] For HFPmn_V2E in Figure 4, the α helix begins at L7. In contrast to the Figure 2 spectra of HFPmn-A6 and HFPtr-A6, which show sharp α and β peaks, the spectrum of HFPmn_V2E-A6 has a single broad peak that indicates structural disorder at A6. In contrast, the spectrum of HFPmn_V2E-L9 does show a sharp α peak.

The A1 residue is placed close to the ^{31}P nuclei in both α and β HFPmn structures because of the substantial $(\Delta S/S_0)^{exp}$ vs τ buildup of the HFPmn-A1 sample. Similar buildup was observed for HFPmn-A14 so the A14 residue in both structures is also placed close to the ^{31}P nuclei. $(\Delta S/S_0)^{\beta}$ of HFPmn-L12 also shows substantial buildup whereas there were much smaller $(\Delta S/S_0)^{\beta}$ buildups for HFPmn-L9 and HFPmn-A6. The HFPmn β strand is therefore represented with shallow curvature and insertion into the membrane. The deepest insertion depth of ~10 Å was chosen because it would result in $(\Delta S/S_0)^{\beta}$ just above the ~12 Å experimental limit for detection of $^{13}CO-^{31}P$ distances. This deepest insertion point is placed near F8 because F8 is between A6 and L9 and is also in the most hydrophobic region of the HFP sequence.

Relative to HFPmn-A1 and HFPmn-A14, there are smaller but still substantial $(\Delta S/S_0)^{exp}$ buildups of HFPtr-A1 and HFPtr-A14. The $(\Delta S/S_0)^{\beta}$ buildups of HFPtr-A6, HFPtr-L9, and HFPtr-L12 are smaller than their respective HFPmn counterparts with no buildup within uncertainty for HFPtr-A6. These results are incorporated into the model of the HFPtr β strand that has higher curvature and deeper insertion than the HFPmn β strand. The deepest insertion depth of ~13 Å was chosen below the detection limit and reflects no buildup for HFPtr-A6.

There are buildups of $(\Delta S/S_0)^{\alpha}$ for HFPmn-A6, HFPmn-L9, and HFPmn-L12 with largest and smallest buildups respectively for HFPmn-L12 and HFPmn-L9. Although the α peak of HFPmn-A14 is not that clearly resolved (Figure 2), there does appear to be substantial dephasing of this α peak. The greatest insertion depth of α helical HFPmn is estimated to be ~9 Å using $\lambda \approx 0.4$ for $\tau = 24$ ms. The variation in $(\Delta S/S_0)^{\alpha}$ with labeled residue is primarily ascribed to rotation on the helical wheel with deepest insertion near L7 and F8 and near F11. There is an overall tilt angle of ~10° for the helix axis relative to the membrane plane. This angle helps to locate the more polar C-terminal residues of HFP closer to the polar membrane headgroups.

As with the $(\Delta S/S_0)^{\beta}$ buildups, the $(\Delta S/S_0)^{\alpha}$ buildups for HFPtr-A6, HFPtr-L9, and HFPtr-L12 are smaller than those of the corresponding HFPmn. There is no $(\Delta S/S_0)^{\alpha}$ buildup for HFPtr-A6 within uncertainty. The α helical HFPtr is therefore more deeply inserted than α helical HFPmn and the greatest insertion depth of ~13 Å reflects no buildup for HFPtr-A6. The same rotational angle is used for the helical wheels of HFPtr and HFPmn, which reflects the identical sequences of the HFP strands. The overall helix tilt angle for HFPtr is ~15°.

The $(\Delta S/S_0)^{\alpha}$ buildups of HFPmn_V2E-L9 and HFPmn_V2E-L12 are generally similar to the $(\Delta S/S_0)^{\alpha}$ buildups of the corresponding HFPtr. The α helical HFPmn_V2E is therefore shown with the same insertion profile as HFPtr but with an α helix that begins at L7 rather than I4. The α helical population is dominant for HFPmn_V2E so the broad signals of the A1, I4, and A6 samples are consistent with a disordered A1-A6 region that precedes the α helix. There are substantial $(\Delta S/S_0)^{exp}$ buildups for the A1, I4, and A6 samples that are reflected in some contact between the A1−A6 region and the phosphate layer. The rotation angle of the helical wheel of HFPtr was also used for the wheel of HFPmn_V2E. However, this HFPmn_V2E angle is not well-constrained by the data. Only the HFPmn_V2E-L9 and HFPmn_V2E-L12 samples have clear α peaks and therefore $(\Delta S/S_0)^{\alpha}$ that constrain the $^{13}CO-^{31}P$ distances.

■ DISCUSSION

Overview. Previous studies using SSNMR as well as other biophysical methods have shown that in membranes with ~0.3 mol fraction cholesterol, HFPmn and HFPtr predominantly form oligomeric antiparallel β sheet structure.[15] In membranes without cholesterol, there is an additional α helical population that is likely monomeric.[14] Both HFPmn and HFPtr induce vesicle fusion for either membrane composition but the fusion is more rapid and extensive with cholesterol.[6,21] Cholesterol changes both membrane physical properties as well as HFP structure, and in our view, it is not yet understood whether one or both of these changes underlie greater fusion.[42] The rate of vesicle fusion induced by HFPtr is ~40 times faster than that of HFPmn fusing membranes with cholesterol and ~15 times faster than HFPmn fusing membranes without cholesterol.

The present study showed that the HFPmn_V2E point mutant induces much less fusion than HFPmn, which is consistent with earlier observations using peptides without the C-terminal solubility tag as well as observations with the whole virus. Earlier SSNMR work also probed β sheet HFP location in membranes with cholesterol and showed that (1) HFPmn_V2E was in the membrane headgroup region and (2) the most apolar A6-L9 region of HFPtr contacted the lipid −CH$_3$ groups at the membrane center, and the A6-L9 region of HFPmn contacted the lipid −CH$_2$− groups midway between the headgroups and membrane center.[15] These data supported insertion of β sheet HFPmn and HFPtr into a single membrane leaflet and a strong correlation between the depth of membrane insertion and fusogenicity. This correlation may be due to the greater lipid disorder associated with deeper insertion and with membranes that are closer to the presumed disordered structure of the fusion transition state with consequent reduced fusion activation energy and more rapid fusion.

One motivation of the present study was better understanding of the structures and membrane locations of HFPmn_V2E, HFPmn, and HFPtr. The membranes did not contain cholesterol and the SSNMR spectra showed that for HFPmn and HFPtr, there were populations of molecules with either α helical or β sheet structure in the A6-L12 region whereas for HFPmn_V2E, these populations were only clearly observed in the L9-L12 region. In the regions closer to the N- or C-termini of the HFPs, the spectra were consistent with more disordered structure. The A6-L12 region is also part of the structured region of α helical HFPmn in detergent. Significant α and β populations of membrane-associated HFP are not an artifact of truncation of the gp41 regions that are C-terminal of the FP. These FP populations have also been observed by SSNMR for constructs that contain regions C-terminal of the FP including two constructs which have most of the rest of the gp41 ectodomain.[2,32]

Similar Membrane Locations of α and β Structures. HFPmn and HFPtr have approximately equal populations of molecules with either α or β structure in the A6-L12 region. For either construct at the same τ value, $(\Delta S/S_0)^{\alpha} \approx (\Delta S/S_0)^{\beta}$, which is interpreted as comparable membrane locations of the α and β structures. Although this similarity has been suggested in earlier studies of HFPmn, we think that the present study provides much more compelling evidence for this similarity through the combination of (1) residue specificity of the SSNMR approach, (2) survey of a large number of residues, and (3) α/β similarity for both HFPmn and for HFPtr.[14,21] For each construct, other data support the fusogenicity of both the

α and β structures.[6] The similar membrane locations of the α and β structures for a given HFP construct support the hypothesis that this location is a key determinant of HFP fusogenicity. Our premise is that HFP with regular secondary structure catalyzes membrane fusion. This premise is supported by a previous study of the rates of HFP binding, HFP β sheet formation, and vesicle fusion, which showed that the rates of binding and β sheet formation were an order of magnitude faster than the rate of vesicle fusion.[43] However, this premise remains controversial.[35,36]

Correlation between Membrane Insertion Depth and Fusogenicity. As noted above, $(\Delta S/S_0)^{\alpha}_{mn} \approx (\Delta S/S_0)^{\beta}_{mn}$ for labeling at A6, L9, or L12 and similarly $(\Delta S/S_0)^{\alpha}_{tr} \approx (\Delta S/S_0)^{\beta}_{tr}$. In addition, $(\Delta S/S_0)^{\alpha}_{mn} \geq (\Delta S/S_0)^{\alpha}_{tr}$ and $(\Delta S/S_0)^{\beta}_{mn} \geq (\Delta S/S_0)^{\beta}_{tr}$, which evidence deeper membrane insertion of HFPtr in both the α and β structures (Figure 4). The vesicle fusion data support more rapid and extensive fusion for α helical HFPtr relative to α helical HFPmn and for β sheet HFPtr relative to β sheet HFPmn so there is a clear correlation between membrane insertion depth and fusogenicity for both structures. Deeper insertion into a single leaflet will likely induce greater perturbation of the surrounding lipids with consequent reduced fusion activation energy and more rapid fusion.

This insertion depth/fusogenicity correlation was previously observed for β sheet HFPmn and HFPtr in membranes with cholesterol.[15] The present study provides further support for this correlation for β sheet HFP structure as well as the new observation that the correlation also holds for α helical HFP structure. These results also support the general hypothesis that membrane location is the key structural determinant of HFP fusogenicity. The observed insertion of the A6−L9 region of α helical HFPmn into the hydrocarbon core of the membrane also correlates with previous LSNMR detection of this region of α helical HFPmn in the hydrocarbon core of the detergent micelle.[7−10]

Deeper membrane insertion of α helical HFPtr relative to α helical HFPmn might reasonably be due to the higher hydrophobicity of three localized HFP strands in HFPtr compared to a single strand for HFPmn. Both β sheet HFPtr and β sheet HFPmn are antiparallel oligomers of HFP strands and deeper insertion of β sheet HFPtr might be due in part to HFPtr oligomers with larger numbers of strands and consequent higher hydrophobicity. An alternate model is different distributions of antiparallel registries for HFPtr and HFPmn with higher populations of hydrophobic registries for HFPtr.

We denote $(\Delta S/S_0)^{\beta,\text{no-chol}}$ for the samples of the present study that lacked cholesterol and denote $(\Delta S/S_0)^{\beta,\text{chol}}$ for samples of an earlier study that contained ~0.3 mol fraction cholesterol.[15] In general, for a given HFPmn-A6, -L9, or -L12 sample and τ value, $(\Delta S/S_0)_{mn}^{\beta,\text{no-chol}} \geq (\Delta S/S_0)_{mn}^{\beta,\text{chol}}$ and the same inequality holds for HFPtr samples, i.e., $(\Delta S/S_0)_{tr}^{\beta,\text{no-chol}} \geq (\Delta S/S_0)_{tr}^{\beta,\text{chol}}$. These inequalities likely reflect deeper HFP insertion in membranes with cholesterol and this deeper insertion could be part of the reason for the more rapid and extensive HFP-induced fusion of vesicles that contain cholesterol.[6,21,32] The deeper insertion of HFPtr in membranes with cholesterol is supported by REDOR-detected contact between the A6 or L9 ^{13}CO nuclei and lipid ^{19}F nuclei located near the membrane center. As noted earlier, HFP ^{13}CO-lipid ^{19}F REDOR was attempted in the present study but the spectral signal-to-noise was too low to provide meaningful contact

information. Relative to membranes lacking cholesterol, there is dilution of ^{31}P nuclei in membranes with cholesterol, which could increase HFP ^{13}CO-lipid ^{31}P distances and decrease $(\Delta S/S_0)^{\text{exp}}$. However, this effect is reduced by "cholesterol condensation", i.e., denser packing of lipids in membranes with cholesterol.[16]

Truncated Helix of HFPmn_V2E. For Figure 2, there are sharp α and β signals for the HFPmn-A6 and HFPtr-A6 spectra and a broader HFPmn_V2E-A6 spectrum. Sharp signals are observed for all constructs that are either L9- or L12-labeled. These data are interpreted to mean distinct populations with either α or β structure in the A6-L12 region for HFPmn and HFPtr and the L9−L12 region of HFPmn_V2E. For membranes with cholesterol, the SSNMR spectra showed predominant sharp β signals for all A6-, L9-, or L12-labeled constructs, which indicates that the β structure is well-defined for all three constructs in the A6−L12 region. For membranes without cholesterol, the difference between the HFPmn_V2E-A6 and the HFPmn-A6 and HFPtr-A6 spectra is therefore interpreted to evidence a loss of N-terminal helicity in HFPmn_V2E (Figure 4). This loss in membranes was not previously observed by LSNMR in detergent where data for both the native and V2E sequences were consistent with continuous α helical structure in the I4-L12 region.[9] Loss of N-terminal helicity was also not observed in molecular dynamics simulations in membranes of ~1 ns duration.[37] In our view, this N-terminal disruption of the helix is plausible as it correlates with the N-terminal location of the V2E mutation.

Unlike the more fusogenic HFPmn and HFPtr, the less fusogenic HFPmn_V2E has a dominant α helical population that is consistent with the results of one earlier infrared study.[19] Greater α population for HFPmn_V2E has also been previously observed in membranes with cholesterol.[15] As previous studies suggest that α structure is less fusogenic than β structure, the lower fusogenicity of HFPmn_V2E may be due in part to its higher α population. Another factor may be coupled loss of N-terminal helicity and change in N-terminal membrane location. Figure 3a shows that $(\Delta S/S_0)^{\text{exp}}$ for HFPmn_V2E-A6 is greater than $(\Delta S/S_0)^{\text{exp}}$ for HFPmn-A6 or HFPtr-A6 whereas Figure 3b shows that $(\Delta S/S_0)^{\alpha}$ for either HFPmn_V2E-L9 or HFPmn_V2E-L12 is comparable or smaller than $(\Delta S/S_0)^{\alpha}$ for the comparably labeled HFPmn or HFPtr. These differences are incorporated into the Figure 4 models of α structure and membrane location. The shorter helix of HFPmn_V2E and lack of membrane insertion of its longer disordered N-terminus may reduce perturbation of the lipid molecules with consequent lower fusogenicity.

Relation to HIV Fusion. The trimeric topology of the three FPs in HFPtr likely reflects their topology in the fusion-active form of trimeric gp41.[1,32] The deep insertion of HFPtr into a single leaflet in both the α and β structures is therefore the most relevant membrane location of the FPs in fusion-active gp41. The trimeric topology and deep insertion of HFPtr correlate to rapid vesicle fusion similar to that observed for the "N70" construct which contains the 70 N-terminal residues of gp41 including the FP and which is likely assembled as trimers.[32,44] N70 is one model for the fusion-active form of gp41. SSNMR spectra of N70 in membranes also show populations of molecules with either α or β FP structures and there is greater β population in membranes with cholesterol similar to the HFP constructs of the present study.[32]

We now consider the relevance of our study to HIV/host cell fusion. We first note that the relative significances of α vs β FP

structures are not yet known for this fusion process. The β structure observed for HFP and N70 may play some role in fusion as both the HIV and host cell membranes contain cholesterol. The HIV membrane is especially cholesterol-rich with a cholesterol:lipid mole ratio ≈0.8.[41] We also note that the rapid intervesicle lipid mixing induced by HFPtr and N70 likely correlates to gp41 FP-induced lipid mixing between the HIV and host cell membranes. This mixing is an early step in the HIV/host cell fusion process and the FP structures and membrane locations of HFPtr likely correspond to FP structures in this early state of gp41.[1,32,40]

CONCLUSIONS

Conclusions from this paper include: (1) the α helical and β sheet structures of membrane-associated HIV fusion peptides have similar membrane locations including insertion into a single membrane leaflet; (2) there is a strong positive correlation between the membrane insertion depth of the peptide and its fusogenicity for both the α helical and β sheet peptide structures; and (3) the reduced fusogenicity associated with the V2E mutation is likely due to a combination of lower β sheet population and a shorter helix with overall less peptide insertion into the membrane. The β sheet fusion peptide may therefore be the most functionally relevant structure for HFPmn-, HFPtr-, and gp41-mediated membrane fusion.

ASSOCIATED CONTENT

Ⓢ Supporting Information

Spectra of the HFPmn-L9 sample over the full ^{13}C chemical shift range and tables of $(\Delta S/S_0)^{exp}$ vs τ. This material is available free of charge via the Internet at http://pubs.acs.org.

AUTHOR INFORMATION

Corresponding Author

*E-mail: weliky@chemistry.msu.edu. Phone: 517-355-9715.

Notes

The authors declare no competing financial interest.

ACKNOWLEDGMENTS

ABBREVIATIONS

DPPC-F5, 1-palmitoyl-2-(5-fluoropalmitoyl)-*sn*-glycero-3-phosphocholine; DPPC-F16, 1-palmitoyl-2-(16-fluoropalmitoyl)-*sn*-glycero-3-phosphocholine; DTPC, 1,2-di-*O*-tetradecyl-*sn*-glycero-3-phosphocholine; DTPG, 1,2-di-*O*-tetradecyl-*sn*-glycero-3-[phospho-(1′-*rac*-glycerol)]; exp, experimental; FP, fusion peptide; gp41, glycoprotein 41; HEPES, *N*-(2-hydroxy-ethyl)-piperazine-*N*′-2-ethanesulfonic acid; HFP, HIV fusion peptide; HFPmn, monomer HIV fusion peptide; HFPmn_V2E, monomer HIV fusion peptide with V2E mutation; HFPtr, trimer HIV fusion peptide; HIV, human immunodeficiency virus; lab, labeled; LSNMR, liquid-state NMR; MAS, magic angle spinning; na, natural abundance; *N*-NBD-PE, *N*-(7-nitro-2,1,3-benzoxadiazol-4-yl)-dipalmitoylphosphatidylethanolamine; *N*-Rh-PE, *N*-(lissamine Rhodamine B sulfonyl)-dipalmitoylphosphatidylethanolamine; POPC, 1-palmitoyl-2-oleoyl-*sn*-glycero-3-phosphocholine; POPG, 1-palmitoyl-2-oleoyl-*sn*-glycero-3-[phospho-(1′-*rac*-glycerol)]; *r*, $^{13}CO-^{31}P$

distance; REDOR, rotational-echo double-resonance; sim, simulated; SSNMR, solid-state NMR

REFERENCES

(1) White, J. M.; Delos, S. E.; Brecher, M.; Schornberg, K. Structures and Mechanisms of Viral Membrane Fusion Proteins: Multiple Variations on a Common Theme. *Crit. Rev. Biochem. Mol. Biol.* **2008**, *43*, 189−219.

(2) Vogel, E. P.; Curtis-Fisk, J.; Young, K. M.; Weliky, D. P. Solid-State Nuclear Magnetic Resonance (NMR) Spectroscopy of Human Immunodeficiency Virus gp41 Protein That Includes the Fusion Peptide: NMR Detection of Recombinant Fgp41 in Inclusion Bodies in Whole Bacterial Cells and Structural Characterization of Purified and Membrane-Associated Fgp41. *Biochemistry* **2011**, *50*, 10013−10026.

(3) Durell, S. R.; Martin, I.; Ruysschaert, J. M.; Shai, Y.; Blumenthal, R. What Studies of Fusion Peptides Tell Us About Viral Envelope Glycoprotein-Mediated Membrane Fusion. *Mol. Membr. Biol.* **1997**, *14*, 97−112.

(4) Nieva, J. L.; Agirre, A. Are Fusion Peptides a Good Model to Study Viral Cell Fusion? *Biochim. Biophys. Acta* **2003**, *1614*, 104−115.

(5) Yang, J.; Prorok, M.; Castellino, F. J.; Weliky, D. P. Oligomeric β-Structure of the Membrane-Bound HIV-1 Fusion Peptide Formed from Soluble Monomers. *Biophys. J.* **2004**, *87*, 1951−1963.

(6) Yang, R.; Prorok, M.; Castellino, F. J.; Weliky, D. P. A Trimeric HIV-1 Fusion Peptide Construct Which Does Not Self-Associate in Aqueous Solution and Which Has 15-Fold Higher Membrane Fusion Rate. *J. Am. Chem. Soc.* **2004**, *126*, 14722−14723.

(7) Chang, D. K.; Cheng, S. F.; Chien, W. J. The Amino-Terminal Fusion Domain Peptide of Human Immunodeficiency Virus Type 1 gp41 Inserts into the Sodium Dodecyl Sulfate Micelle Primarily as a Helix with a Conserved Glycine at the Micelle-Water Interface. *J. Virol.* **1997**, *71*, 6593−6602.

(8) Chang, D. K.; Cheng, S. F. Determination of the Equilibrium Micelle-Inserting Position of the Fusion Peptide of gp41 of Human Immunodeficiency Virus Type 1 at Amino Acid Resolution by Exchange Broadening of Amide Proton Resonances. *J. Biomol. NMR* **1998**, *12*, 549−552.

(9) Morris, K. F.; Gao, X. F.; Wong, T. C. The Interactions of the HIV gp41 Fusion Peptides with Zwitterionic Membrane Mimics Determined by NMR Spectroscopy. *Biochim. Biophys. Acta* **2004**, *1667*, 67−81.

(10) Jaroniec, C. P.; Kaufman, J. D.; Stahl, S. J.; Viard, M.; Blumenthal, R.; Wingfield, P. T.; Bax, A. Structure and Dynamics of Micelle-Associated Human Immunodeficiency Virus gp41 Fusion Domain. *Biochemistry* **2005**, *44*, 16167−16180.

(11) Gabrys, C. M.; Weliky, D. P. Chemical Shift Assignment and Structural Plasticity of a HIV Fusion Peptide Derivative in Dodecylphosphocholine Micelles. *Biochim. Biophys. Acta* **2007**, *1768*, 3225−3234.

(12) Li, Y. L.; Tamm, L. K. Structure and Plasticity of the Human Immunodeficiency Virus gp41 Fusion Domain in Lipid Micelles and Bilayers. *Biophys. J.* **2007**, *93*, 876−885.

(13) Qiang, W.; Bodner, M. L.; Weliky, D. P. Solid-State NMR Spectroscopy of Human Immunodeficiency Virus Fusion Peptides Associated with Host-Cell-Like Membranes: 2D Correlation Spectra and Distance Measurements Support a Fully Extended Conformation and Models for Specific Antiparallel Strand Registries. *J. Am. Chem. Soc.* **2008**, *130*, 5459−5471.

(14) Qiang, W.; Weliky, D. P. HIV Fusion Peptide and Its Cross-Linked Oligomers: Efficient Syntheses, Significance of the Trimer in Fusion Activity, Correlation of β Strand Conformation with Membrane Cholesterol, and Proximity to Lipid Headgroups. *Biochemistry* **2009**, *48*, 289−301.

(15) Qiang, W.; Sun, Y.; Weliky, D. P. A Strong Correlation between Fusogenicity and Membrane Insertion Depth of the HIV Fusion Peptide. *Proc. Natl. Acad. Sci. U. S. A.* **2009**, *106*, 15314−15319.

(16) Qiang, W.; Yang, J.; Weliky, D. P. Solid-State Nuclear Magnetic Resonance Measurements of HIV Fusion Peptide to Lipid Distances

Reveal the Intimate Contact of Beta Strand Peptide with Membranes and the Proximity of the Ala-14-Gly-16 Region with Lipid Headgroups. *Biochemistry* **2007**, 46, 4997−5008 PMCID: 2631438..

(17) Zheng, Z.; Yang, R.; Bodner, M. L.; Weliky, D. P. Conformational Flexibility and Strand Arrangements of the Membrane-Associated HIV Fusion Peptide Trimer Probed by Solid-State NMR Spectroscopy. *Biochemistry* **2006**, 45, 12960−12975.

(18) Zheng, Z.; Qiang, W.; Weliky, D. P. Investigation of Finite-Pulse Radiofrequency-Driven Recoupling Methods for Measurement of Intercarbonyl Distances in Polycrystalline and Membrane-Associated HIV Fusion Peptide Samples. *Magn. Reson. Chem.* **2007**, 245, S247−S260.

(19) Pereira, F. B.; Goni, F. M.; Nieva, J. L. Liposome Destabilization Induced by the HIV-1 Fusion Peptide Effect of a Single Amino Acid Substitution. *FEBS Lett.* **1995**, 362, 243−246.

(20) Schmick, S. D.; Weliky, D. P. Major Antiparallel and Minor Parallel Beta Sheet Populations Detected in the Membrane-Associated Human Immunodeficiency Virus Fusion Peptide. *Biochemistry* **2010**, 49, 10623−10635.

(21) Lai, A. L.; Moorthy, A. E.; Li, Y. L.; Tamm, L. K. Fusion Activity of HIV gp41 Fusion Domain Is Related to Its Secondary Structure and Depth of Membrane Insertion in a Cholesterol-Dependent Fashion. *J. Mol. Biol.* **2012**, 418, 3−15.

(22) Agirre, A.; Flach, C.; Goni, F. M.; Mendelsohn, R.; Valpuesta, J. M.; Wu, F. J.; Nieva, J. L. Interactions of the HIV-1 Fusion Peptide with Large Unilamellar Vesicles and Monolayers. A Cryo-Tem and Spectroscopic Study. *Biochim. Biophys. Acta* **2000**, 1467, 153−164.

(23) Haque, M. E.; Koppaka, V.; Axelsen, P. H.; Lentz, B. R. Properties and Structures of the Influenza and HIV Fusion Peptides on Lipid Membranes: Implications for a Role in Fusion. *Biophys. J.* **2005**, 89, 3183−3194.

(24) Gullion, T. Introduction to Rotational-Echo, Double-Resonance NMR. *Concepts Magn. Reson.* **1998**, 10, 277−289.

(25) Toke, O.; Maloy, W. L.; Kim, S. J.; Blazyk, J.; Schaefer, J. Secondary Structure and Lipid Contact of a Peptide Antibiotic in Phospholipid Bilayers by REDOR. *Biophys. J.* **2004**, 87, 662−674.

(26) Doherty, T.; Waring, A.; Hong, M. Membrane-Bound Conformation and Topology of the Antimicrobial Peptide Tachyplesin I by Solid-State NMR. *Biochemistry* **2006**, 45, 13323−13330.

(27) Murphy, O. J., 3rd; Kovacs, F. A.; Sicard, E. L.; Thompson, L. K. Site-Directed Solid-State NMR Measurement of a Ligand-Induced Conformational Change in the Serine Bacterial Chemoreceptor. *Biochemistry* **2001**, 40, 1358−1366.

(28) Graesser, D. T.; Wylie, B. J.; Nieuwkoop, A. J.; Franks, W. T.; Rienstra, C. M. Long-Range ^{19}F-^{15}N Distance Measurements in Highly-^{13}C, ^{15}N-Enriched Solid Proteins with ^{19}F-Dephased Redor Shift (Fresh) Spectroscopy. *Magn. Reson. Chem.* **2007**, 45, S129−S134.

(29) Tristram-Nagle, S.; Nagle, J. F. Lipid Bilayers: Thermodynamics, Structure, Fluctuations, and Interactions. *Chem. Phys. Lipids* **2004**, 127, 3−14.

(30) Xie, L.; Ghosh, U.; Schmick, S. D.; Weliky, D. P. Residue-Specific Membrane Location of Peptides and Proteins Using Specifically and Extensively Deuterated Lipids and ^{13}C-^{2}H Rotational-Echo Double-Resonance Solid-State NMR. *J. Biomol. NMR* **2013**, 55, 11−17.

(31) Freed, E. O.; Delwart, E. L.; Buchschacher, G. L., Jr.; Panganiban, A. T. A Mutation in the Human Immunodeficiency Virus Type 1 Transmembrane Glycoprotein gp41 Dominantly Interferes with Fusion and Infectivity. *Proc. Natl. Acad. Sci. U. S. A.* **1992**, 89, 70−74.

(32) Sackett, K.; Nethercott, M. J.; Epand, R. F.; Epand, R. M.; Kindra, D. R.; Shai, Y.; Weliky, D. P. Comparative Analysis of Membrane-Associated Fusion Peptide Secondary Structure and Lipid Mixing Function of HIV gp41 Constructs That Model the Early Pre-Hairpin Intermediate and Final Hairpin Conformations. *J. Mol. Biol.* **2010**, 397, 301−315.

(33) Gabrys, C. M.; Yang, R.; Wasniewski, C. M.; Yang, J.; Canlas, C. G.; Qiang, W.; Sun, Y.; Weliky, D. P. Nuclear Magnetic Resonance Evidence for Retention of a Lamellar Membrane Phase with Curvature in the Presence of Large Quantities of the HIV Fusion Peptide. *Biochim. Biophys. Acta* **2010**, 1798, 194−201.

(34) Tristram-Nagle, S.; Chan, R.; Kooijman, E.; Uppamoochikkal, P.; Qiang, W.; Weliky, D. P.; Nagle, J. F. HIV Fusion Peptide Penetrates, Disorders, and Softens T-Cell Membrane Mimics. *J. Mol. Biol.* **2010**, 402, 139−153.

(35) Reichert, J.; Grasnick, D.; Afonin, S.; Buerck, J.; Wadhwani, P.; Ulrich, A. S. A Critical Evaluation of the Conformational Requirements of Fusogenic Peptides in Membranes. *Eur. Biophys. J.* **2007**, 36, 405−413.

(36) Wadhwani, P.; Reichert, J.; Burck, J.; Ulrich, A. S. Antimicrobial and Cell-Penetrating Peptides Induce Lipid Vesicle Fusion by Folding and Aggregation. *Eur. Biophys. J.* **2012**, 41, 177−187.

(37) Kamath, S.; Wong, T. C. Membrane Structure of the Human Immunodeficiency Virus gp41 Fusion Domain by Molecular Dynamics Simulation. *Biophys. J.* **2002**, 83, 135−143.

(38) Maddox, M. W.; Longo, M. L. Conformational Partitioning of the Fusion Peptide of HIV-1 gp41 and Its Structural Analogs in Bilayer Membranes. *Biophys. J.* **2002**, 83, 3088−3096.

(39) Promsri, S.; Ullmann, G. M.; Hannongbua, S. Molecular Dynamics Simulation of HIV-1 Fusion Domain-Membrane Complexes: Insight into the N-Terminal gp41 Fusion Mechanism. *Biophys. Chem.* **2012**, 170, 9−16.

(40) Munoz-Barroso, I.; Durell, S.; Sakaguchi, K.; Appella, E.; Blumenthal, R. Dilation of the Human Immunodeficiency Virus-1 Envelope Glycoprotein Fusion Pore Revealed by the Inhibitory Action of a Synthetic Peptide from gp41. *J. Cell Biol.* **1998**, 140, 315−323.

(41) Brugger, B.; Glass, B.; Haberkant, P.; Leibrecht, I.; Wieland, F. T.; Krasslich, H. G. The HIV Lipidome: A Raft with an Unusual Composition. *Proc. Natl. Acad. Sci. U. S. A.* **2006**, 103, 2641−2646.

(42) Bloom, M.; Evans, E.; Mouritsen, O. G. Physical Properties of the Fluid Lipid-Bilayer Component of Cell Membranes: A Perspective. *Q. Rev. Biophys.* **1991**, 24, 293−397.

(43) Buzon, V.; Padros, E.; Cladera, J. Interaction of Fusion Peptides from HIV gp41 with Membranes: A Time-Resolved Membrane Binding, Lipid Mixing, and Structural Study. *Biochemistry* **2005**, 44, 13354−13364.

(44) Sackett, K.; Wexler-Cohen, Y.; Shai, Y. Characterization of the HIV N-Terminal Fusion Peptide-Containing Region in Context of Key gp41 Fusion Conformations. *J. Biol. Chem.* **2006**, 281, 21755−21762.

9859

dx.doi.org/10.1021/jp312845w | *J. Phys. Chem. A* 2013, 117, 9848−9859

Supporting Information for "Solid-State Nuclear Magnetic Resonance Measurements of HIV Fusion Peptide ^{13}CO to Lipid ^{31}P Proximities Support Similar Partially Inserted Membrane Locations of the α Helical and β Sheet Peptide Structures"

Charles M. Gabrys, Wei Qiang, Yan Sun, Li Xie, Scott D. Schmick, and David P. Weliky

Department of Chemistry, Michigan State University, East Lansing, MI, 48824
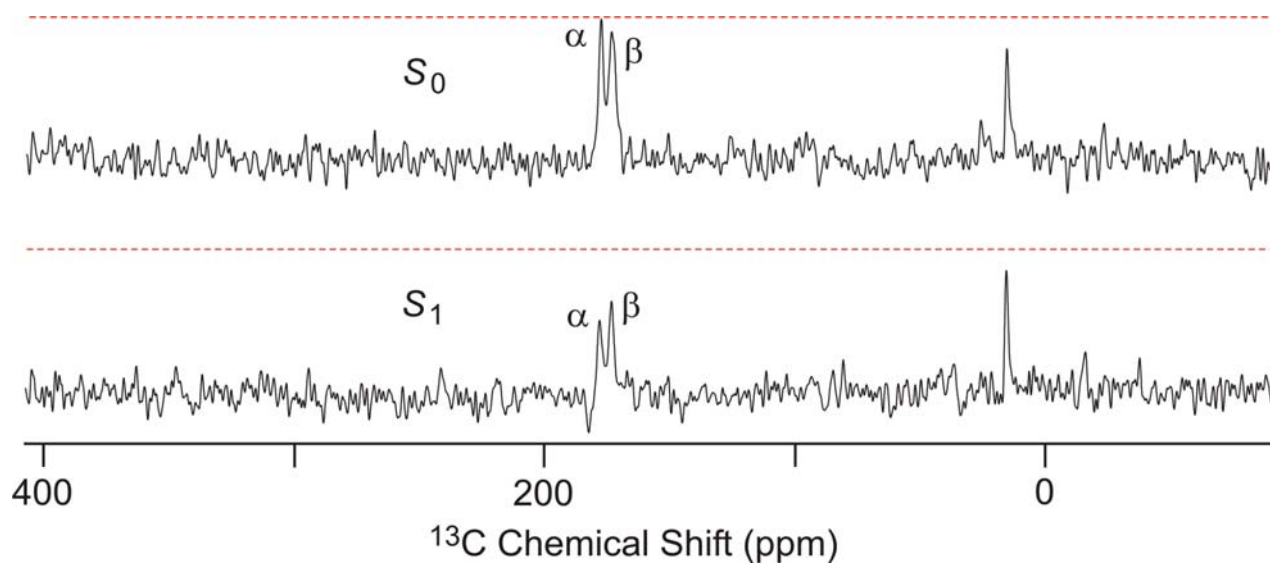
Figure S1. ^{13}C-^{31}P REDOR S_0 and S_1 spectra at 24 ms dephasing time of the sample containing HFPmn that was ^{13}CO labeled at L9. The α and β signals are respectively due to the HFPmn populations with either α helical or β sheet structure at L9. The dashed red lines are at the peak intensity of the S_0 α signal. The signals at 15 ppm are due to natural abundance ^{13}CH$_3$ nuclei of the lipid molecules. Both the S_0 and S_1 spectra were processed with 100 Hz Gaussian line broadening and baseline correction and are the sum of 24704 scans.

1

Table S1. Full peak $(\Delta S/S_0)^{exp} \times 100$ [a]

Construct	Labeling	Dephasing time (ms)				
		2 ms	8 ms	16 ms	24 ms	32 ms
HFPmn_V2E	A1	5 (9)	−11 (16)	−12 (13)	73 (24)	
	I4	16 (10)	−9 (8)	20 (5)	27 (6)	41 (5)
	A6	1 (5)	15 (6)	46 (6)	52 (5)	
	L9	2 (4)	11 (4)	14 (5)	22 (4)	27 (7)
	L12	−5 (7)	10 (4)	23 (4)	43 (2)	51 (3)
	A14	−7 (11)	12 (7)	20 (7)	21 (7)	
HFPmn	A1	11 (7)	49 (6)	63 (7)	81 (7)	
	A6	3 (5)	15 (5)	27 (7)	18 (5)	28 (6)
	L9	3 (6)	12 (4)	28 (4)	42 (4)	
	L12	12 (6)	21 (5)	47 (6)	77 (6)	
	A14	7 (7)	21 (5)	46 (4)	67 (4)	74 (5)
HFPtr	A1	−15 (7)	21 (7)	42 (10)	43 (5)	
	I4	4 (12)	10 (11)	40 (7)	52 (3)	
	A6	4 (5)	10 (4)	1 (4)	7 (3)	2 (4)
	L9	8 (5)	5 (6)	19 (4)	37 (4)	
	L12	−1 (10)	8 (7)	22 (9)	37 (6)	
	A14	7 (6)	18 (6)	39 (8)	54 (5)	

[a] Each number in parentheses is one standard deviation based on measurement of spectral noise.

Table S2. α and β peak $(\Delta S/S_0)^{exp} \times 100$ [a,b]

Construct	Labeling	Peak	Dephasing time (ms)				
			2 ms	8 ms	16 ms	24 ms	32 ms
HFPmn_V2E	L9	α	4 (4)	1 (5)	12 (6)	17 (4)	24 (7)
		β	6 (9)	20 (12)	24 (17)	39 (12)	
	L12	α	–2 (11)	16 (7)	18 (7)	35 (3)	44 (4)
		β	–1 (11)	4 (8)	26 (8)	47 (4)	53 (5)
HFPmn	A6	α	7 (12)	29 (10)	44 (15)	10 (10)	52 (11)
		β	2 (6)	3 (7)	16 (9)	26 (5)	13 (8)
	L9	α	7 (11)	15 (8)	37 (8)	45 (7)	
		β	1 (9)	9 (7)	20 (6)	35 (7)	
	L12	α	1 (13)	25 (11)	56 (12)	68 (10)	
		β	11 (8)	25 (7)	36 (11)	77 (10)	
HFPtr	A6	α	2 (9)	5 (6)	0 (7)	10 (5)	9 (7)
		β	11 (8)	10 (6)	2 (7)	3 (5)	–2 (7)
	L9	α	7 (9)	2 (10)	19 (5)	32 (5)	
		β	7 (8)	11 (9)	17 (6)	38 (7)	
	L12	α	14 (13)	11 (11)	28 (16)	25 (13)	
		β	–22 (22)	2 (13)	20 (13)	42 (9)	

[a] Integration was done using a 2 ppm window centered at the peak shift.

[b] Each number in parentheses is one standard deviation based on measurement of spectral noise.